International Journal of ISSI, Vol. 14 (2017), No. 2, pp. 1-8

Micro Laser Welding of AISI 430 Ferritic Stainless Steel: Mechanical Properties, Magnetic Characterization and Texture Evolution

H. Mostaan [*1] , F. Nematzadeh [2]

[1, 2] *Department of Materials and Metallurgical Engineering, Faculty of Engineering, Arak University, Arak 38156-8-8349, Iran*

Abstract

In the present work, a high power Nd:YAG laser has been employed to weld AISI 430 ferritic stainless steel thin sheets. Optical microscopy was used to study the microstructural evolutions during laser welding. Tensile test and microhardness measurement were employed in order to investigate the mechanical behaviors of the welds. Also, vibrational sample magnetometry was used for characterizing magnetic properties. Texture evolution during laser welding of AISI 430 stainless steel was also studied and a correlation was made between texture evolution and magnetic properties of the welded samples. The effects of welding cycle on the mechanical properties of the laser welds in terms of fracture strength and microhardness profile were discussed. It was found that the magnetic properties of the welded samples experience significant decrease due to the formation of large grains in the fusion zone which are oriented in an unfavorable direction. The results showed that the grain size of the base metal increases from 17 μm up to 92 μm after laser welding. Also, base metal had a dominant γ-fiber, some α-fiber components and also rotated cube texture component. After laser welding, the intensity of cube texture component was diminished and while α and γ-fibers were completely disappeared. These phenomena also led to a decrease in fracture strength of the welded samples.

Keywords: Laser welding; Texture evolution; AISI 430; Magnetic properties; Mechanical properties.

1. Introduction

Ferritic stainless steels are characterized by lower cost, higher thermal conductivity, smaller linear expansion and better resistance to chloride stress corrosion cracking, atmospheric corrosion and oxidation, compared to austenitic stainless steels [1, 2]. In the last few decades, the ferritic stainless steel variety is becoming important in the stainless steel market [3]. They exhibit lower expansion coefficient compared to austenitic stainless steels, which is a great advantage when temperature cycling resistance is needed. Ferritic stainless steels serve as good substitute for austenitic stainless steels in various applications which are not limited to automotive exhaust components, especially the upstream part of the exhaust line (manifold, down-pipe, and converter shell) etc. [4].

Ferritic stainless steels can have good soft magnetic properties showing high permeability, low coercive force, low residual magnetic flux density, and high magnetic saturation flux density. These steels also have high electrical resistivity which is essential to minimize eddy current losses in a.c. magnet applications [5]. The combination of these properties has meant that ferritic and stainless steels have been used in a broad range of magnetic applications [6, 7]. They can be used in fuel injectors and fuel pumps on automobiles, in relays, motors, and generators, and they also have potential for using in nuclear power plants [5].

For many of these applications welding is a major route adopted for fabrication of components made by these alloys [8]. Although it finds application in a very wide area, it is restricted as a structural material because the fusion welding of the grade is associated with several challenges. A major concern in the industrial application of ferritic stainless steel is the loss of ductility and impact toughness in the weld section due to the intense welding heat which induces grain coarsening [9]. Excessive grain growth can be avoided, of course, by using lower welding heat inputs. Another problem in welding of ferritic stainless steels is about formation of sigma-phase (σ-phase). Several undesirable intermetallic phases such as r-phase may occur when stainless steels are exposed to 650–850 °C for a period of time. σ-phase has a great hardness, approximately 700–800 HV, and a tough structure. To prevent the σ-phase, stainless steels must not be preheated over 400 °C. Another solution is

**Corresponding author*
Email: H-mostaan@araku.ac.ir
Address: Department of Materials and Metallurgical Engineering, Faculty of Engineering, Arak University, Arak 38156-8-8349, Iran
1. Assistant Professor
2. Assistant Professor

stainless steels must be cooled very quickly after welding [10].The above-mentioned effects during fusion welding can be severely altering magnetic properties of material which in some cases the changes are unfavorable.

So, it is of prime importance to choose an appropriate welding process and also, to control welding process parameters in order to minimize the adverse effects of welding on the magnetic and mechanical properties of welded samples. Conventional resistance welding and gas tungsten arc welding techniques are no longer suited for joining small, delicate, and ultra-thin metallic parts because these processes cause excessive melting and unacceptable heat-affected-zones. Laser welding is a highly attractive joining technology widely applied in the automotive, aerospace, energy, electronic, and medical industries [11, 12]. The advantages of laser beam welding include precise energy control, repeatability and flexibility, low thermal distortion, small heat-affected zones, high welding speed, and the ability to produce good-strength welds. Moreover, a pulsed laser provides better performance than the continuous welding lasers by transferring a minimum amount of energy to components with high precision, thereby generating the minimum size of the HAZ and very small distortion [13-15]. Accordingly, laser welding of ferritic stainless steel such as AISI 430, can be an appropriate choice of joining process.

Since there are no results in the literature regarding this particular kind of weld joint or similar industrial applications, the first purpose of this study was to investigate the influence mechanism of laser welding on the mechanical and magnetic properties of AISI 430 stainless steel sheets. Finally, in this context, texture evolution and its relationship with properties is explored. The authors believe that the obtained results in this work would help with exploiting full advantages of these alloys.

2. Material and Experimental Procedure

2. 1. Material

The base metal (BM) used in this study was AISI 430 (X6Cr17, material number 1.4016) ferritic stainless steel with the composition presented in Table 1. The BM was in annealed condition and the thickness of BM was 0.4 mm. The maximum load for fracture of BM was about 1000 N. The sheets were cut and machined into rectangular welding samples, 200 mm long, 50 mm wide and 0.4 mm thick which were longitudinally lap welded using a laser welding machine.

Table. 1. Chemical composition of the studied alloy (in wt. %).

Elements	Fe	C	Cr	Mn	Mo	Si	S
wt.%	81	0.12	16	1.25	0.58	1	0.06

2. 2. Welding process

Fig. 1 schematically illustrates the experimental set-up used in this study. The control of the gap size during welding was crucial.

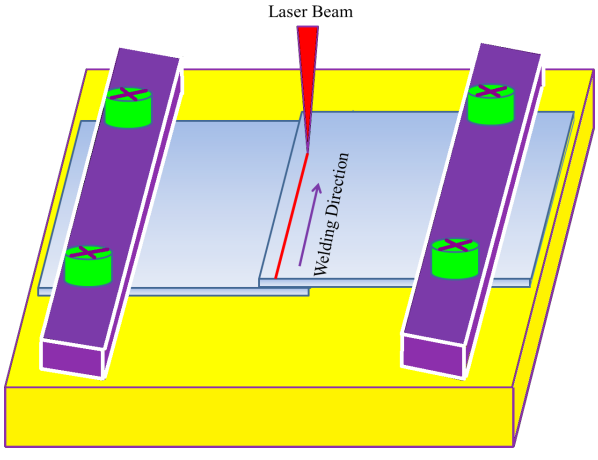

Fig. 1. Schematic illustration of laser welding set-up.

Hence, the end of sheet was fixed into a fixture to prevent any gap between the sheets and minimize weld distortion. The laser beam irradiates the specimen surfaces under the constant welding conditions (see Table. 2).

Table. 2. Welding parameters used in this study.

Pulse shape	**Rectangular**
Focal length (mm)	100
Beam spot size (mm)	0.15
Pulse repetition rate (Hz)	50
Laser wavelength (nm)	1064

A charge–coupled–device (CCD) camera was placed directly above the welding platform in order to monitor the welding process. A pulsed Nd:YAG laser with a maximum mean power of 800W in near TEM00 mode was used for welding the magnetic sheets.Argon shielding gas was provided at a flow rate of 10 l/min to prevent the effects of moisture and contaminations that

Table. 3. Test conditions used in this study.

Symbol	Lamping Current (A)	Pulse Duration (ms)	Travel Speed (mm/min)
Sample A	187.5	12.5	6
Sample B	195	17.5	6

otherwise causes porosity and cracking and also to suppress the plasma formation during welding. In order to study the effect of heat input on the welds, two samples were welded according to the conditions listed in Table. 3. The schematic diagram of laser welding process is shown in Fig. 1.
Fig. 2 shows a weld sample in lap joint configuration.

Fig. 2. Close view of welded sample in butt joint configuration.

2. 3. Metallurgical Analysis

Samples for the metallographic examinations have been prepared by polishing successively in 80, 120, 220, 320, 400, 1200, 1600, 2000 grade emery papers to remove the scratches. Then each of the samples was polished by diamond paste. After performing the polishing with diamond paste each of the samples was ready for etching. The composition of the etchant was dilute aqua regia (15 ml HCl, 5 ml HNO_3, and 100 ml H_2O at room temperature). Microstructure of the welded area was analyzed using optical microscope (OM; Olympus BX50). X-ray diffraction (XRD) measurements were carried out using a Bruker 2D system, with Cr k_α radiation to determine the texture of the welded samples. The incomplete experimental pole figure data (pole figure of (110) and (200) planes) were used to calculate orientation distribution function (ODF) plots and inverse pole figures (IPFs) by TexTools software (RestMatCo.).

A series of experiments was performed in order to study the mechanical properties of the laser welded lap joints. Micro-hardness survey was made on flat metallographic specimens across the joints and top to the bottom in the weld using Vickers microhardness testing machine (Wolpert Wilson 402-MVD) at 100 gf loads with 10 s dwell time. For each zone, the microhardness measurements were taken from three points at an interval of four times the indenter size to avoid the effects of localized strain hardening in the vicinity of the indentation. Finally, the averages of the three measurements were reported. A tensile shear test was carried out in order to evaluate the strength of the laser welded lap joints. For each experiment, eight coupons were used in the tensile shear test. All the test coupons were cut with an abrasive wire cutting machine per the ASTM standard.

The room temperature magnetic hysteresis (B-H) loops of the welded samples were measured by vibrating sample magnetometer (VSM, Meghnatis Kavir Kashan Co), vibration frequency: 82.5 Hz; Max. Field: 20 KGauss; Moment range: 0.0001 emu to 50 emu. A 5×5 mm^2 specimen was cut from the welded samples in order to measure the magnetic properties.

3. Results and Discussion

3. 1. Microstructural evolutions

Fig. 3 shows a typical OM micrograph of the base metal (BM) after heat treatment. As the investigated AISI 430 was cold rolled and annealed, the fully ferritic microstructure along with some carbide can be found in the BM microstructure. The carbides were evenly distributed throughout the matrix. It was observed that the average grain size of AISI 430 base metal was about 17 µm.

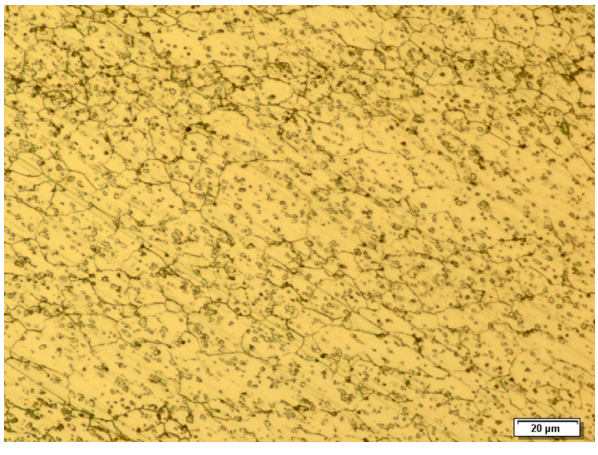

Fig. 3. OM micrograph of BM (AISI 430).

The XRD pattern of the AISI 430 base metal is shown in Fig. 4. As shown, only two major peaks of ferritic structure i.e. (110) and (200) at 2θ=69.15 and 106.55. No other peak can be observed in the XRD pattern which indicates that the base metal is single phase. Itshould be noted that X-ray cannot detect phases thattheir volume fraction is lower than about 5 percent [16]. So, it can be said that the absence of carbide peaks in the XRD pattern is due to low volume fraction of this phase in the microstructure.

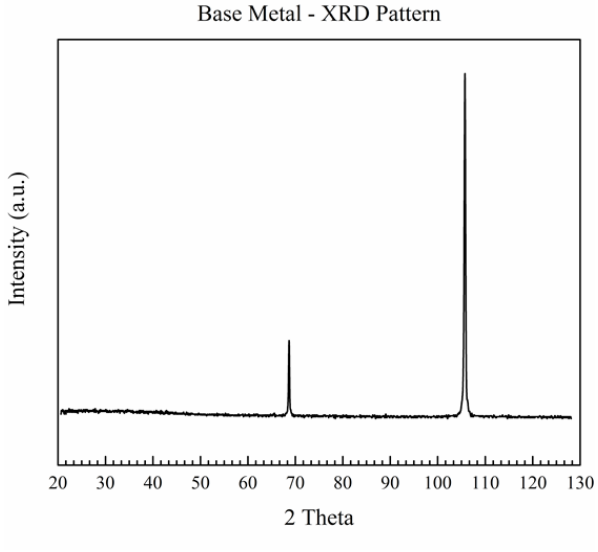

Fig. 4. XRD pattern of the AISI 430 base metal.

Optical micrographs showing the microstructures of weld zone, fusion boundary and HAZ is presented in Fig. 5.

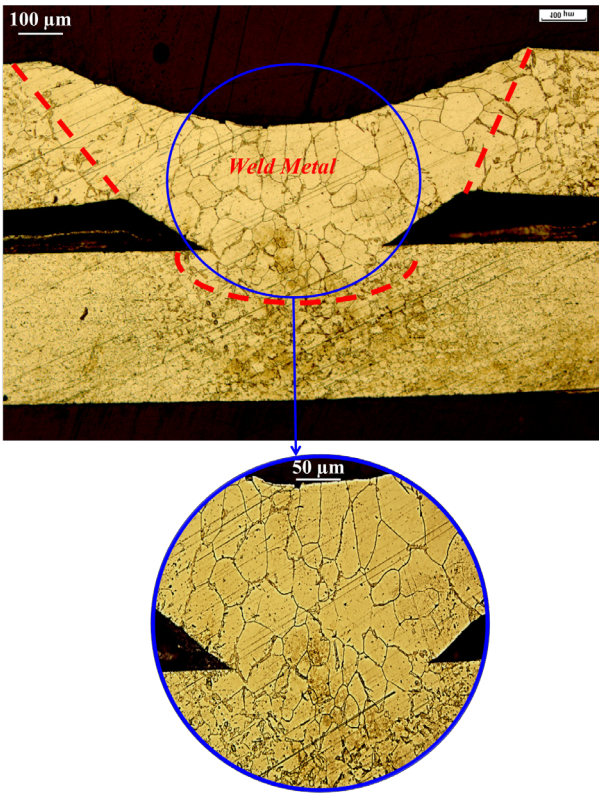

Fig. 5. Cross section of lap joint between two AISI 430 sheets made with pulsed Nd:YAG laser welding.

The microstructure shows that melting started at the surface irradiates by the laser beam and the molten pool grows continuously to axial and radial axis. The weld region is distinguished by the dashed lines. Areas near the heat source of the upper sheet were heated to higher temperatures and thus expanded more than areas away from the heat source or regions of the lower sheet. After the sheets cooled to the initial temperature, the final deformation remained. Like the material heated by the laser beam, the irradiance did not cause the material reach its boiling point; no significant amount of surface material was removed. The microscopic examination of the cross section also indicated that the weld pool morphology is essentially symmetrical about the axis of the laser beam. A hemispherical weld bead is formed in a similar manner to conventional arc fusion welding processes [17-19]. This symmetry at the top and bottom suggests a steady fluid flow in the weld pool; as can be seen, no welding cracks can be found in the weld region, this may be partly due to the good crack resistance of the AISI 430 base metal and the correct welding parameters. Moreover, no discontinuities are observed in the weld metal. It demonstrates the efficiency of the shielding gas in preventing oxidation, large porosities and gas inclusions. It should be mentioned that all specimens were laser-welded in the conduction mode: direct heating and energy transmission. The mechanism of direct heating involves absorption of the beam energy by the material surface of the top sheet and subsequent transfer of energy into the surrounding material by conduction. The microstructural analysis shows that the average grain size in the weld metal are considerably larger than the base metal and has been grown up to about 92 µm after laser welding. It is worthy to note that no carbide has been formed in the weld metal and weld metal has a single phase ferritic structure. XRD pattern from the weld metal is shown in Fig. 6 which indicates single phase state of the weld metal.

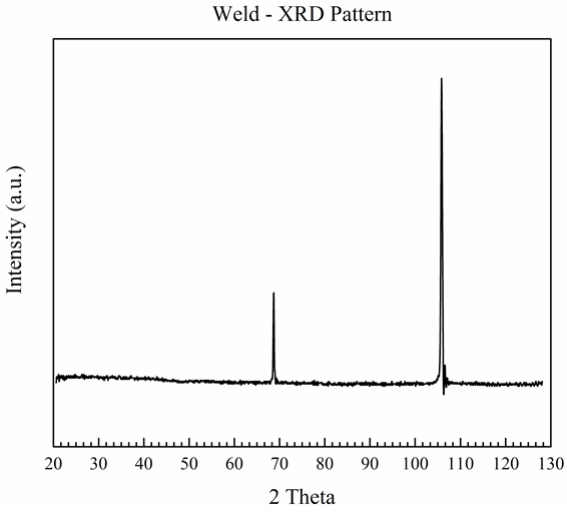

Fig. 6. XRD pattern of the AISI 430 weld metal.

This structure of ferrite has a polygonal morphology. This ferritic microstructure forms at the highest austenite transformation temperatures and the ferrite crystals or grains are nucleated as grain-boundary allotriomorphs and grow away from austenite grain boundaries to form equiaxed grains. Growth of polygonal ferrite is controlled by rapid substitutional atom transfer across partially coherent or disordered austenite-ferrite interfaces and long-range diffusion of carbon atoms rejected from the growing ferrite. In addition, no columnar or cellular grains can be seen in the vicinity of weld metal interface.

Another important feature in the microstructural evolutions during laser welding of AISI 430 stainless steel is the formation of three distinct regions in the HAZ region including the coarse grained HAZ (CGHAZ), fine-grained HAZ (FGHAZ) and intercritical HAZ (ICHAZ). The typical microstructure of the as-welded HAZ regions is shown in Fig. 7. The non-equilibrium HAZ clearly consists of three different sub-zones, including the CGHAZ, FGHAZ and ICHAZ.

Fig. 8 shows a schematic fusion welding peak temperature profile and the typical microstructure in various heat-affected zones of the weldment. Due to the high heating and cooling rates, a few phase transformations occur in the HAZ, including diffusive austenitic phase transformation on-heating, grain coarsening and

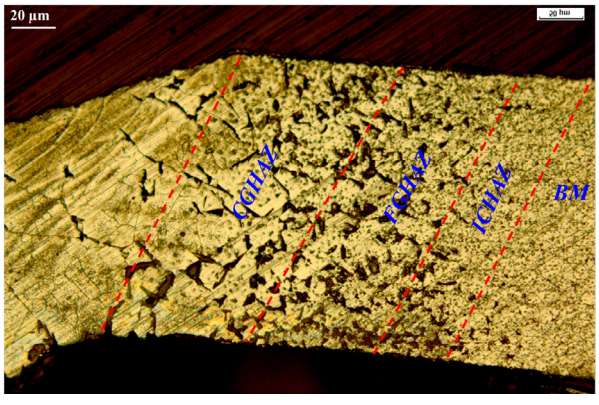

Fig. 7. Microstructure of the HAZ in an as-welded AISI 430 stainless steel showing CGHAZ, FGHAZ and BM.

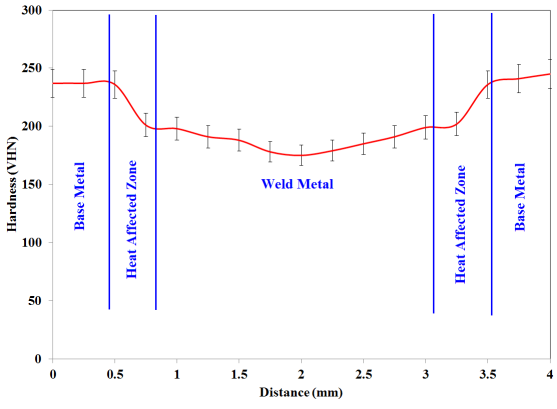

Fig. 9. Curve presenting hardness changes in the cross section of the AISI 430 joint made using laser beam welding.

precipitate dissolution or coarsening during the thermal cycle. According to Fig. 8, it should be noted that the peak temperature of CGHAZ and FGHAZ regions is higher than the upper critical temperature (A_3). Due to the high peak temperatures (much higher than A_3), the BM transforms to coarse austenitic grains along with the dissolution of former $M_{23}C_6$ in the CGHAZ during the heating cycles. It is reported that the austenitic grains quickly grow because of the decreased pining force from the dissolved precipitates. Former ferrite transforms to austenite without further growth, because the FGHAZ is exposed to a peak temperature T_p just above A_3 and a short soaking time. Precipitates, especially coarse $M_{23}C_6$ carbides, do not get sufficient time to be completely dissolved [10].

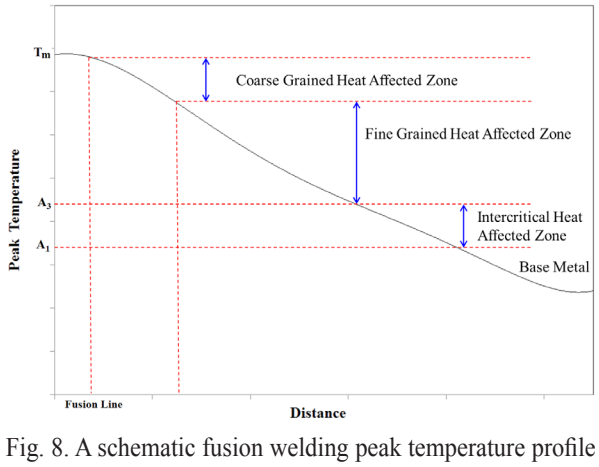

Fig. 8. A schematic fusion welding peak temperature profile in the heat-affected zone (HAZ) of a typical weldment.

3. 2. Mechanical properties

A microhardness distribution map in Fig. 9 is reconstructed based on the Vickers hardness values measured from the cross-sectional weldment (From BM to weld metal). Average hardness values of the different sub-regions are presented. The measurements were performed from the weld axis in both directions, with distances between measurement points amounting to 0.04 mm each. The measurement line was located at the half of the depth of a weld.

The cross-sectional hardness measurements of the joint made using a laser beam revealed that the laser weld joint underwent grain coarsening leading to a significant decrease in hardness of the weld material and that of the HAZ. The decrease in hardness was confirmed by the results of microscopic metallographic tests revealing the presence of coarse grains in almost the entire volume of the weld metal and HAZ. The lowest hardness (174 HVN) was measured in the center of weld metal which undergoes maximum temperature.

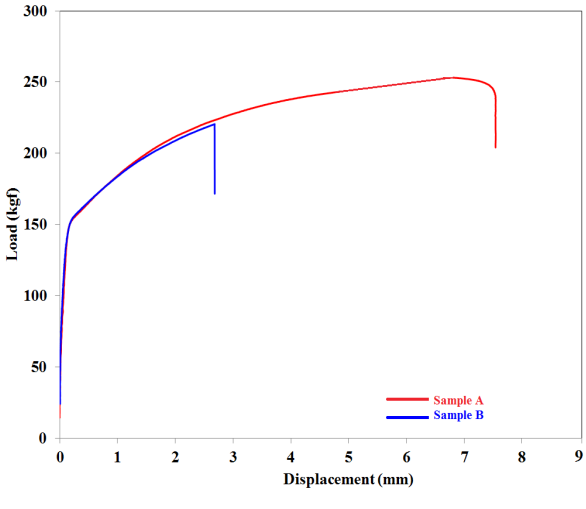

Fig. 10. Load–displacement curves of the specimens with different heat inputs.

Tensile tests were performed at room temperature. Each joint was subjected to three tensile tests. The results of the tensile tests involving the joints made using laser beam with different parameters are shown in Fig. 10 (sample A and sample B). The tensile test results revealed that in each case, i.e. while welding using the high energy or low energy laser beam, the specimens subjected to tensile tests ruptured in the weld metal. In

each case, the strength of the welded joint is lower than that of the base metal. The tensile strength values of the specimens amounted to 221 (kgf) as regards the joint welded using the high energy laser beam (sample B) and approximately 252 (kgf) in case of the joint welded using lower energy laser beam (sample A).

Decrease in tensile strength in the sample B in comparison to sample A can be attributed to the formation of larger grains (and formation of a larger weak area due to the laser welding) because of higher heat input in sample B.

3. 3. Texture evolutions and magnetic properties changes

In this section, texture evolution during welding will be discussed. It has been shown that the magnetic properties are sensitive to the texture components. So, after presentation the results of texture evolution, the correlation between magnetic properties and texture evolution will be discussed in details.

A detailed analysis of textural evolution has been presented using orientation distribution functions (ODFs). The ODF plots separate the components that partially overlap in the pole figures, allowing for a more unambiguous comparison of the individual components and fibers. The ODFs are presented as plots of constant φ_2 sections with isointensity contours in Euler space defined by the Euler angles φ_1, φ, and φ_2. The texture evolution of the base metal and weld metal is shown as ODFs in Fig. 11.

To facilitate the texture analysis, the ideal orientations of some typical texture components and the corresponding texture fibers commonly found in bcc metals are presented in Fig. 12.

Comparing Fig. 11 and 12 reveals that texture of the base metal in Fig. 11 (a) has a dominant -fiber, some α-fiber components and also rotated cube texture component. γ-fiber represents components with crystallographic texture of <111>//ND. But after laser welding, the cube texture however has been diminished when α and γ-fiber completely disappears.

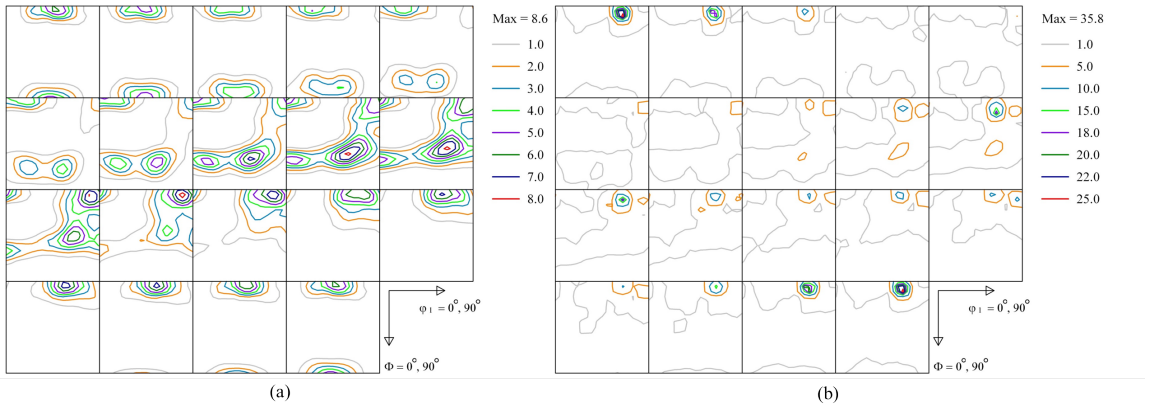

Fig. 11. ODFs of the (a) base metal and (b) weld metal.

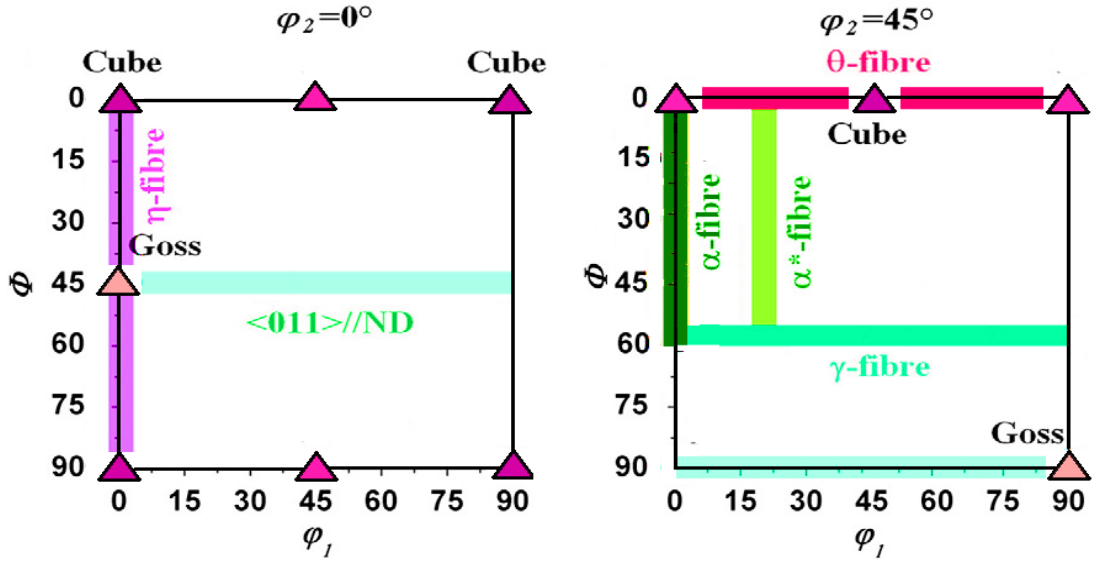

Fig. 12. The ideal orientation positions for the main texture components ($\varphi_2 = 0^\circ$ *and* 45°).

As shown above, the grain orientation of the base metal remarkably changes and a new texture is produced upon welding. This is important since residual flux density (Br) can be severely affected by orientation of grains. In addition, it has been shown that considerable microstructural evolution was occurred during laser welding of AISI 430 stainless steel. The values of coercivity and residual flux density of the base metal and welded samples (sample A and sample B) are shown in Fig. 13. It should be mentioned that coercivity (Hc) and residual flux density are the main magnetic characteristics in soft magnetic materials such as AISI 430 stainless steel. So, it is aimed to investigate the change mechanisms of these two magnetic properties. As can be seen in Fig. 13, the coercivity of base metal is about 9.42 Oe. This value has been decreased after laser welding down to 7.72 and 6.02 Oe for sample A and sample B respectively. The value of Hc provides information about the difficulty of moving magnetic domain walls, and it is highly sensitive to the microstructure. Hc is sensitive to microstructure and for ferritic stainless steels depend on the grain size, chromium carbide inclusions size and their distribution. These inclusions inhibit domain wall motion leading to harder magnetic properties. The influence of inclusions on the coercive force of ferromagnetic materials has been studied by many researchers [5]). Domain wall motion is resisted by inclusions for three reasons. Firstly, the wall area and therefore wall energy is reduced when it resides on an inclusion (the ‘‘surface tension’’ effect). Secondly, the intersection of a wall at an inclusion site allows a rearrangement of magnetic poles which reduces the energy of the poles [5]). Thirdly, when the inclusion is several times the wall thickness (~0.1 mm for iron), spiked closure domains form around the inclusion. These domains act to reduce the free pole energy at the inclusion, but they also inhibit wall motion dependence of Hc on the grain size implies that grain boundaries serve as pinning sites for the magnetic domain wall. The pinning effect of the grain boundaries has been investigated by the Lorentz electron microscopy. The Lorenz electron microscopy observations revealed that a considerable amount of magnetic domain walls lie along the grain boundaries and are curved at intersecting points of grain boundaries, indicating that grain boundaries act as pinning sites for magnetic domain wall movement. Considering Figs. 3 and 5, it is clear that the grain size of base metal (17 µm) is much lower than that of weld metal (92 µm). On the other hand, it was shown that chromium carbide inclusions are present in the microstructure of base metal; while no chromium carbide inclusion is formed in the weld metal due to the high cooling rate during laser welding. Taking all these changes (formation of larger grains in the weld metal and diminishing of chromium carbide inclusions in the weld metal) into account, decrease in Hc of welded specimens can be clearly interpreted. In other words, by an increase in grain size and decrease in volume fraction of chromium carbide inclusion, the obstacles against domain wall movement have decreased and hence the values of Hc for welded sample have been decreased.

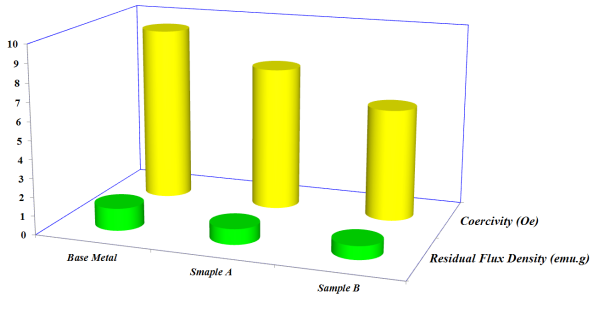

Fig. 13. The values of coercivity and residual flux density in the base metal and welded samples (sample A and sample B).

As shown in Fig. 13, the value of Br of AISI 430 stainless steel is decreased after laser welding. The value of Br is mainly affected by orientation of grains. In case of materials which have a BCC crystal structure such as

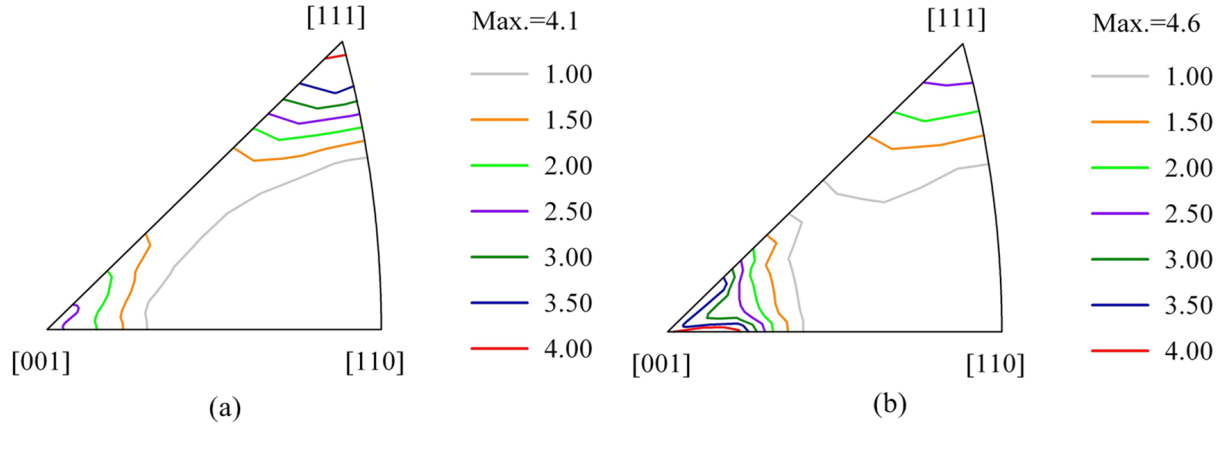

Fig. 14. Inverse pole figures for (a) base metal and (b) a typical welded sample.

AISI 430 stainless steel, the <100> directions are the ones of easy magnetization while the <111> directions require more energy for saturation of the magnetic polarization. Br is maximum when the material exhibited a perfect <111> fiber texture 20). Figs. 14 (a) and (b) show the inverse pole figures (IPFs) for base metal and welded area respectively. As can be seen, there is a strong <111> fiber texture in the base metal, while the intensity of this fiber texture has been decreased in the weld area. The predominant fiber texture in the weld area is <100> which is an easy axis of magnetization. So, it can be said that decrease in the value of Br caused by laser welding is due to the formation of stronger <100> texture in the weld area. In other words, in this condition, magnetic domains easily can rotate in the absence of magnetic field and consequently the Br value decreases.

4. Conclusions

AISI 430 ferritic stainless steel thin sheets have been welded using pulsed Nd:YAG laser without filler wire. OM observation was used to investigate the microstructure in various regions. Also, texture, magnetic properties and mechanical properties of welded sample were studied. On the basis of the present results, the following conclusions can be reached.

- Laser welding of AISI 430 stainless steel led to formation of large exuiaxed grains in weld area which their size was about 5.5 times larger than that of base metal.
- Three distinct regions in the HAZ region including the CGHAZFGHAZ) and ICHAZ were formed in the HAZ of laser welded AISI 430 stainless steel.
- XRD analysis showed that the weld area was in single phase state.
- Tensile test results showed that all of the welded samples fractured from weld area indicating lower strength of this area.
- The texture of base metal which consisted of strong γ-fiber, some α-fiber components and rotated cube texture, changed after laser welding. But after laser welding, the cube texture has been diminished when α and γ-fiber completely disappears.
- VSM analysis showed that there was a noticeable decrease in magnetic properties values for welded area of the samples. The increase in grain size and also the absence of preferred orientation parallel to the harder magnetization axis were identified as major parameters affecting the magnetic properties.

References

[1] G. Mallaiah, A. Kumar, P. Ravinder Reddy and G. Madhusudhan Reddy: Mater. Des., 36(2012), 443.
[2] I. Mészáros: Mater. Sci. Forum., 473(2005), 231.
[3] M.O.H. Amuda and S. Mridha: Mater. Des., 47(2013), 365.
[4] K.D. Ramkumar, A. Chandrasekhar, A.K. Singh, S. Ahuja, A. Agarwal, N. Arivazhagan and A.M. Rabel: J. Manuf., Process., 20(2015), 54.
[5] P. Oxley, J. Goodell and R. Molt: J. Magn. Magn. Mater., 321(2009), 2107.
[6] L. Battistini, R. Benasciutti and A. Tassi: J. Magn. Magn. Mater., 133(1994), 603.
[7] M. B. Bilgin and C. Meran: Mater. Des., 33(2012), 376.
[8] G. Mallaiah, P. R. Reddy and A. Kumar: Procedia. Mater. Sci., 6(2014), 1740.
[9] M. O. H. Amuda and S. Mridha: Mater. Des., 35(2012), 609.
[10] S. Kou: Welding Metallurgy, John Wiley & sons, (2003), 322.
[11] R. K. Leary, E. Merson, K. Birmingham, D. Harvey and R. Brydson: Mater. Sci. Eng. A., 527(2010), 7694.
[12] J. F. Tu and A.G. Paleocrassas: J. Mat. Proc. Tech., 211(2011), 95.
[13] H. Liao and Z. Chen: Int. J. Adv. Manuf. Technol., 67 (2012), 1015.
[14] Y. Zhou: Microjoining and nanojoining, Woodhead Publishing, Cambridge, 2008.
[15] Z. Li and G. Fontana: J. Mat. Proc. Tech., 74(1998), 174.
[16] F. Mirakhorli, F. Malek Ghaini and M. J. Torkamany: J. Mater. Eng. Perform., 21(2012), 2173.
[17] W. Chen and P. Molian: Int. J. Adv. Manuf. Technol. 39(2007), 889.
[18] V. Ventrella, J. Berretta and W. De Rossi: Phys. Procedia., 39(2012), 569.
[19] V. A. Ventrella, J.R. Berretta and W. de Rossi: J. Mater. Process. Technol., 210(2010), 1838.
[20] R. Berretta, W. De Rossi, D. Martins, I. Alves, D. Almeida, N. Dias and V. Junior: Opt. Lasers Eng., 45(2007), 960.
[21] J. J. Sidor, K. Verbeken, E. Gomes, J. Schneider, P. Rodriguez and L.A.I. Kestens: Mater. Charact., 71(2012), 49.